

Demonstrating hydrogen production from ammonia using lithium imide – powering a small proton exchange membrane fuel cell

Hazel MA Hunter^{1*}, Joshua W Makepeace², Thomas J Wood¹, O Simon Mylius³, Mark G Kibble¹,
Jamie B Nutter¹, Martin O Jones¹ and William IF David^{1,2}

¹ISIS Facility, STFC Rutherford Appleton Laboratory, Harwell Campus, Didcot, OX11 0QX, UK.

²Inorganic Chemistry Laboratory, University of Oxford, South Parks Road, Oxford, OX1 3QR, UK

³Arcola Energy Ltd, 24 Ashwin Street, Dalston, London E8 3DL, U.K.

Abstract (<200 words)

Accessing the intrinsic hydrogen content within ammonia, NH_3 , has the potential to play a very significant role in the future of a CO_2 -free sustainable energy supply. Inexpensive light metal imides and amides are effective at decomposing ammonia to hydrogen and nitrogen ($2\text{NH}_3 \rightarrow 3\text{H}_2 + \text{N}_2$), at modest temperatures, and thus represent a low-cost approach to on-demand hydrogen production. Building upon this discovery, this paper describes the integration of an ammonia cracking unit with a post-reactor gas purification system and a small-scale PEM fuel cell to create a first bench-top demonstrator for the production of hydrogen using light metal imides.

Keywords

Ammonia cracking, demonstrator, hydrogen production, PEM fuel cell, lithium imide

Introduction

Environmentally benign, sustainable and economically favourable alternatives to fossil fuels are required if the ever increasing demand for energy worldwide is to be satisfied, while addressing the global impact of a changing climate. In this regard, hydrogen is considered as a promising fuel and energy vector. However, its safe and effective storage remains a key scientific and technological challenge that must be overcome before widespread adoption can be realised. One route to working with hydrogen is to consider liquid ammonia as an approach to storing hydrogen.

Ammonia, NH_3 , is an attractive, ubiquitous and sustainable energy vector if its intrinsic hydrogen content can be accessed for use. Among hydrogen storage candidates, ammonia has one of the highest volumetric ($121 \text{ kg H}_2 \text{ m}^{-3}$ at 10 bar) and gravimetric (17.8 wt%) hydrogen densities and it can be liquefied under relatively mild conditions (<10 bar at room temperature). In addition, its widespread use as an industrial chemical (and fertilizer feedstock) means that the safety hazards are well understood, the handling protocols are defined and documented, and distribution networks already exist – all key considerations if ammonia (as a hydrogen energy vector) is to be adopted in transport and off-grid applications. With nitrogen and water as clean combustion products and with physical properties similar to liquid petroleum gas, ammonia is, in many ways, the ideal non-carbon hydrocarbon.

Indeed ammonia-coal gas mixtures were used as the motor fuel [1] for the Belgian bus fleet during the straitened times of World War II. From 1943 up to the end of the war in 1945, these buses carried passengers for tens of thousands of miles without incident, in a real demonstration of the use of ammonia as an automotive fuel in standard internal combustion engines. More recently, Thomas and Parks have described [2] ammonia as having the potential for use as an energy carrier, particularly in the transition to a hydrogen economy. However, in addition to safety concerns, they identified both the size and cost of current ammonia cracking units and their successful integration with a proton exchange membrane (PEM) fuel cell as potential showstoppers when considering the use of ammonia for on-board vehicular hydrogen storage. This paper addresses these challenges.

We have recently shown [3, 4, 5] that light metal imides and amides define a new class of catalyst for the effective and efficient decomposition of NH_3 into H_2 and N_2 (equation 1), and that this represents a low-cost approach to on-demand hydrogen production.



Thus integrating an ammonia decomposition reactor based on a light metal imide-amide catalyst into a small-scale power generation system provides an opportunity to illustrate and assess the practicality of this innovative hydrogen production method and to address, in part, the concerns of Thomas and Parks [2].

For this work we selected a fuel cell as the small-scale power generating unit, however the choice of fuel cell critically influences the design of the overall system. Although a number of types of fuel cell exist, this work focussed upon low temperature, high efficiency stacks which when assembled within a complete, fully insulated, system have the potential to deliver net energy gains. Specifically, the two relevant types are alkaline fuel cells (AFCs) and PEM fuel cells. AFCs are partially ammonia compatible [6], and have a long standing reputation having been used [7] on the Apollo space missions, but currently are not readily available for purchase. Instead, a PEM fuel cell was selected because this technology is considered to be the leading low-temperature route for power generation for use with hydrogen fuel. PEM fuel cells can also be bought off-the-shelf and do not require significant lab-based infrastructure modifications for testing (unlike internal combustion engines). Moreover, because PEM fuel cells are ammonia intolerant [8] and can be irreparably damaged if more than 100 ppb NH_3 is present in the inlet gas stream, a reliable and robust gas purification method was needed to ensure that no ammonia entered the PEM fuel cell.

For this work, the complete system comprised an ammonia gas supply, an ammonia cracking reactor, a post-reactor gas purification column and a 100 W PEM fuel cell, with associated gas and electrical handling. The technological challenges that were encountered when assembling this demonstrator are discussed in detail.

Experimental

System description

An overview of the experimental set-up, including a photograph of the whole system, is shown in Fig. 1, with more detailed schematic descriptions given in Fig. 2.

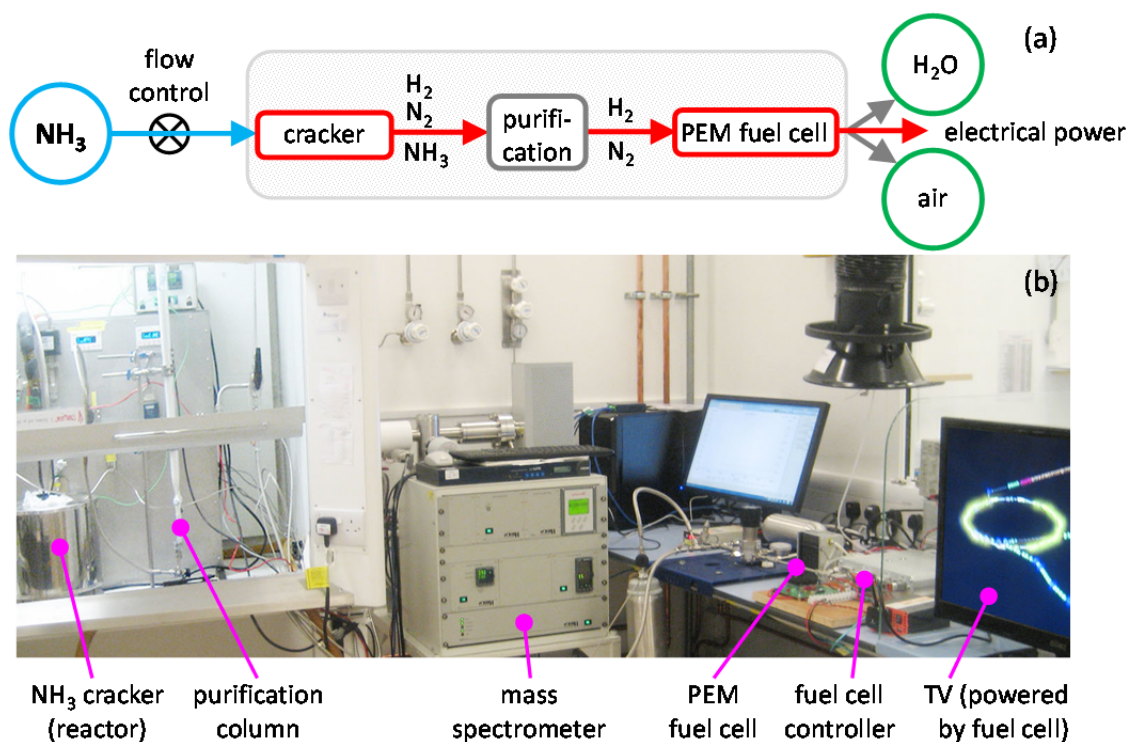


Fig. 1: Experimental set-up (a) system overview and (b) annotated photo.

The NH_3 decomposition reactions were performed in simple cylindrical flow reactors (316 stainless steel) of internal volume 21.3 cm^3 . As described [3, 4] previously, the reactor was fitted with an inlet gas pipe running from the lid to 10 mm from the base of the reactor with a thermocouple monitoring the internal temperature at 5 mm from the base of the reactor. NH_3 (99.98%, SIP Analytical) or argon (99.998%, BOC) gas was supplied to the reactor *via* a custom-designed gas control panel and the exhaust gas stream was passed through a column of anhydrous MgCl_2 before being quantitatively analysed by a Hiden Analytical HPR-20 mass spectrometer. Gas flow inputs were mediated by a mass flow controller (HFC-302, Teledyne Hastings Instruments) and the hydrogen-containing outlet gas flow monitored by a mass flow meter (HFM-300, Teledyne Hastings Instruments). Microfibre gas filters (Parker 05-11-BS, retain 99.99% $\geq 0.01 \mu\text{m}$ particles) were fitted to ensure that the gas streams were particulate-free throughout. Gas flows were recorded in standard cubic centimetres per minute (sccm) and the reactor temperature and system pressure were also logged.

Typically to run the system 1.0 g lithium imide (Li_2NH , the fine powder catalyst) was loaded and sealed into the reactor in an argon-filled glove box, and the reactor connected to the gas panel and heated at $5^\circ \text{C min}^{-1}$ under flowing argon to 585°C . Once stable at 585°C , the gas was switched to NH_3 and the system operated at this constant temperature while varying the NH_3 inlet flow (60–300 sccm) in order to produce sufficient hydrogen to operate the fuel cell at the desired power output. Testing was performed under autogenous pressure, up to 2.0 bar in the reactor and purification column, which was sufficient to deliver the ~ 0.5 bar overpressure needed to run the fuel cell. As reported [3,4] previously, ammonia conversion efficiencies were calculated using a customised computer program, which removes background contributions and determines the ammonia signal as a percentage of the total signal.

To create the ammonia-scavenging purification system, two 19 mm i.d. chromatography columns were filled with anhydrous magnesium chloride, MgCl_2 , powder ($\geq 98\%$, Sigma-Aldrich) and connected in-line (and in parallel to each other) to the reactor and gas control panel. Typically, these columns contained

130–150 g MgCl_2 filled to an initial height of 550–600 mm, with the air in each column purged by flowing argon through the powder for 30 minutes. Some compaction of the powder (4–12%) occurred as the gas was switched from argon to NH_3 and the system pressurised to the ~ 2 bar operating conditions. For one test, a bypass option was set up around the purification column, to allow collection of baseline NH_3 conversion measurements. Also, when required, thermal images were captured using a Fluke Ti20 imaging camera.

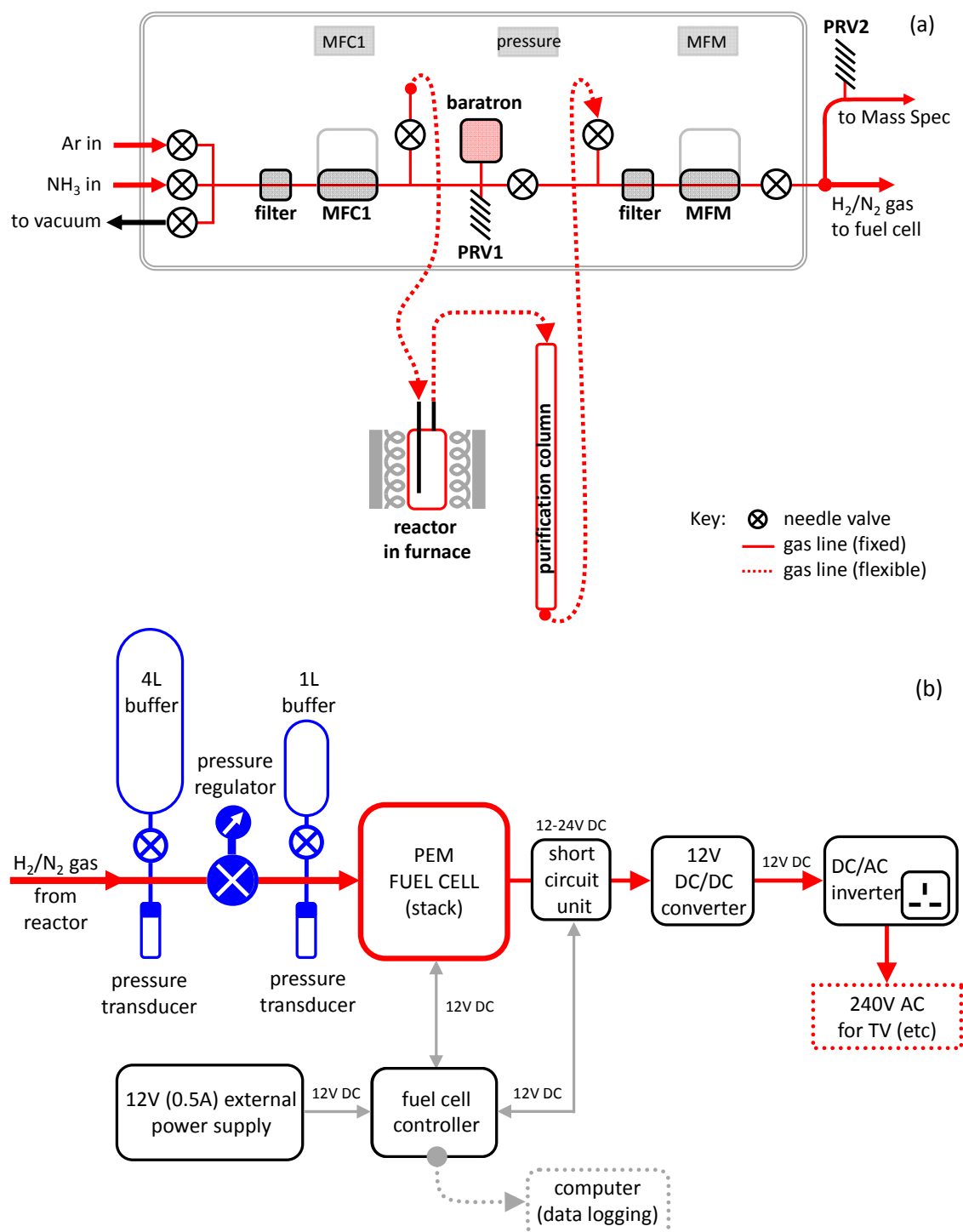


Fig. 2: Detailed schematics for (a) the control and monitoring set-up for producing and purifying hydrogen gas from ammonia [where MFC1 = mass flow controller, MFM = mass flow meter, PRV = pressure relief valve (PRV1 = 5 bar working pressure, PRV2 = 2 bar working pressure)], and (b) the downstream gas and electrical wiring layout for operating and testing the 100 W PEM fuel cell [where the external supply

powers the fuel cell controller, stack valves and short circuit unit only, and all 0 V are shown as common together].

Downstream of the gas control panel, the hydrogen-containing gas was directed into a gas-handling system connected to the fuel cell. This comprised a 4 litre buffer volume, a gas regulator and a 1 litre buffer volume before reaching the supply valve and fuel cell stack. Pressure transducers were connected in-line to allow monitoring of the gas pressures throughout the gas handling system.

The hydrogen-containing gas was supplied to the anode of the semi-integrated low temperature PEM fuel cell (Horizon Fuel Cell Technologies H-100, 100 W, 20 cells). This self-humidifying air-cooled open cathode stack has an active cell area of 22.5 cm^2 . Its membrane electrode assembly is composed of a 0.3 mm thick gas diffusion layer, a serpentine anode flow-field geometry and has a $15 \text{ }\mu\text{m}$ thick ion exchange membrane loaded with platinum at 0.15 and 0.50 mg cm^{-2} on the anode and cathode, respectively. A custom-built fuel cell controller was used to operate the fuel cell from a computer *via* a serial interface. Further electrical circuitry was connected to the fuel cell in order to convert the variable output voltage ($12\text{--}24 \text{ V}$) into a regulated, useable voltage (12 V) to power a device. Specifically, high efficiency components were chosen to minimise the amount of power lost through heat with a peripheral circuit board designed in-house to accommodate a 12 V DC/DC converter (Traco Power TEP 160-2412WIR). A DC/AC inverter (Mercury IMS-150, 150 W soft start modified sine wave inverter) was linked in series to enable a digital LED television to be plugged in and powered by the electricity generated from the fuel cell. Additionally, an external 12 V (0.5 A) supply was required to power the stack valves of the fuel cell, the controller circuitry and the integrated cooling fan (when necessary), however, this 12 V supply did not deliver power to the DC/AC inverter and thus did not power any attached device. A logging function, within the controller, enabled real-time monitoring of the operation of the fuel cell stack when running. The short circuit unit was used as a fail-safe device.

Catalyst preparation

The Li_2NH catalyst powder [9] was prepared in-house by grinding 1.59 g lithium nitride (Li_3N , $>99.5\%$, Aldrich) and 2.41 g lithium amide (LiNH_2 , 95% , Aldrich) together ($1:1$ molar ratio) in an argon-filled glove box, before transferring to a reactor connected to the gas control panel and heating under 25 sccm argon flow at $270 \text{ }^\circ\text{C}$ for 14 hours. The purity of the resultant pale grey powder ($\sim 4 \text{ g}$) was checked by powder X-ray diffraction (XRD) and found to be $>93\%$, with impurities of unreacted Li_3N or oxidised material (i.e. sample that has oxidised upon exposure to moisture during the XRD measurement, identified as Li_2O ; see SI).

Characterisation instrumentation

The gas species were quantitatively analysed by a Hiden Analytical HPR-20 mass spectrometer (Quantitative Gas Analysis, QGA) equipped with MASsoft v7 software and calibrated with a certified gas mixture of composition $10\% \text{ NH}_3$, $67.5\% \text{ H}_2$ and $22.5\% \text{ N}_2$. The mass-to-charge (m/z) values routinely monitored in multi-ion detection mode were $2 (\text{H}_2)$, $17 (\text{NH}_3)$, $18 (\text{H}_2\text{O})$, $28 (\text{N}_2)$, $32 (\text{O}_2)$ and $40 (\text{Ar})$.

The thermogravimetric analysis measurements were collected using a Netzsch STA449 F3 Jupiter DSC-TGA using aluminium pans with pierced lids, and analysed using Netzsch Proteus Thermal Analysis software (v6.1.0). Approximately 15 mg of powdered sample was heated at $5 \text{ }^\circ\text{C min}^{-1}$ under 20 ml min^{-1} flowing N_2 gas, with the mass, temperature and calorimetric characteristics of the sample recorded simultaneously.

Results and Discussion

Ammonia Cracking

The catalyst development programme built upon the initial realisation [4] that the inexpensive bulk chemical sodium amide, NaNH_2 , catalyses the ammonia decomposition reaction, and, in a simple flow cell, this reaction is as effective as the current state-of-the-art transition metal-based catalysts. Our subsequent experiments have shown that imide-forming amides are also highly active, with lithium imide-amide showing [3] superior activity per unit mass than sodium amide.

Further investigation into the properties of ammonia decomposition with respect to catalyst quantity, inlet flow and reaction temperature are necessary to begin to optimise the reactor component of the overall demonstrator system. Fig. 3a confirms that the presence of 0.5 g LiNH_2 catalyst generates superior ammonia conversion, at 500 °C, to that of both 0.5 g NaNH_2 and an empty (blank) reactor. This is true at flows up to 500 sccm. Although the overall conversions are less than 97%, if the temperature is increased to 550 °C then more than 98% of the ammonia is converted into hydrogen and nitrogen at flows of up to 200 sccm, and if the flow is increased to 500 sccm the 0.5 g LiNH_2 catalyst still converts 77% of the ammonia, Fig. 3b.

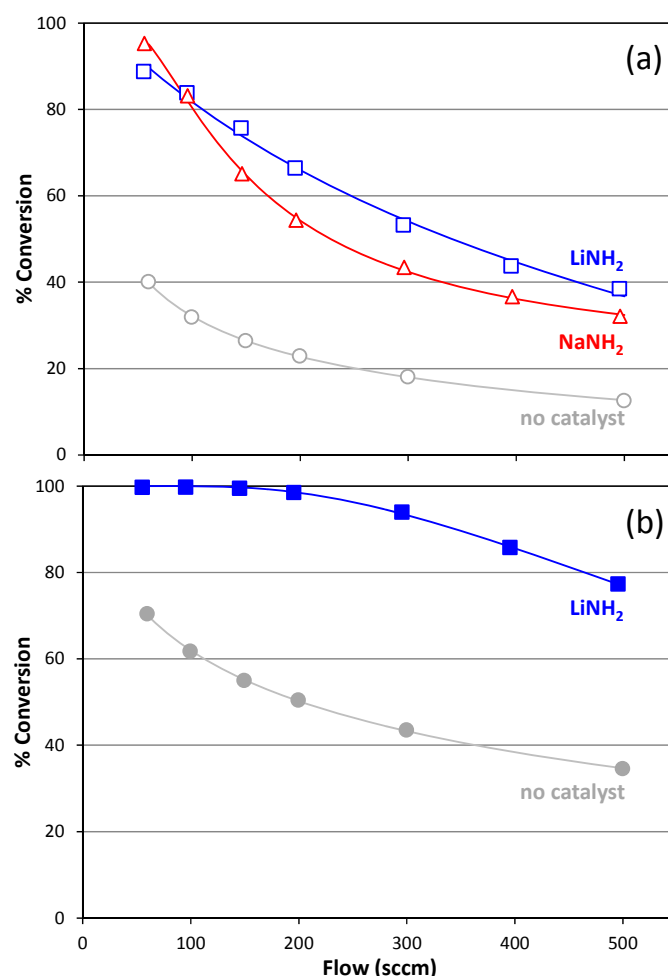


Fig. 3: Ammonia conversion *versus* flow comparison for the empty (blank) reactor (circles) and with 0.5 g NaNH_2 (triangles) or 0.5 g LiNH_2 (squares) at (a) 500 °C and (b) 550 °C. The data are shown fitted [4] to a stretched exponential function.

While promising, an effective demonstrator system requires both high flow and high conversion in order to minimise the level of ammonia scavenging required in the post-reactor gas purification step. Furthermore,

knowing that within this Li-N-H system, ammonia fulfils a 'mediator' role [10] in the lithium amide (LiNH_2) to lithium imide (Li_2NH) desorption of hydrogen, it was decided to investigate the catalyst performance from an initial lithium imide standpoint. The data collected for 1.0 g Li_2NH contained within the reactor at 585 °C are shown in Fig. 4, in comparison to that of the empty (blank) reactor. It clearly shows that the presence of Li_2NH enhances the ammonia decomposition reaction and that more than 99% ammonia decomposition can be achieved at flows of up to 200 sccm, and at least 89% conversion at 500 sccm. Crucially, lithium imide can also be kept solid during the reaction, improving the ability to contain the catalyst material (a significant technological challenge with NaNH_2) within the simple flow reactor. A reaction temperature of 585 °C was chosen as, in the presence of ammonia, it ensures that the catalyst remains solid and a high level of ammonia decomposition is achieved. The reaction temperature is critical for effective ammonia decomposition in the Li-N-H system, given that the catalyst stoichiometry adapts to the reaction conditions [3] and is in dynamic flux with the incoming ammonia molecule. The internal reactor temperatures decrease as the flow increases, indicating that heat is drawn out of the reactor by the gas flow coupled to the endothermic ammonia decomposition reaction. The presence of 1.0 g catalyst enhances this heat loss phenomenon, presumably because more ammonia decomposition occurs and the reaction is endothermic. While further catalyst/reactor optimisation can be undertaken, the Li_2NH result is sufficiently promising to enable the creation of a first demonstrator that showcases this new hydrogen production technology.

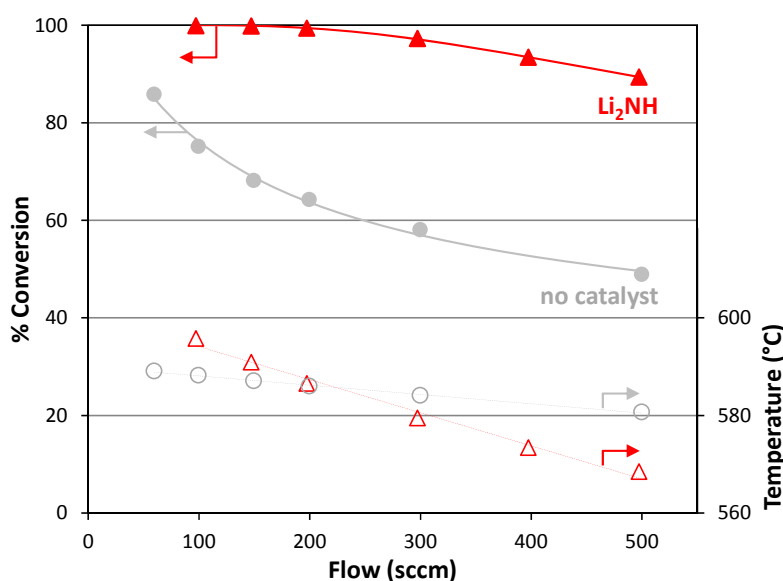


Fig. 4: Ammonia conversion *versus* flow comparison for the empty (blank) reactor (grey circles) and with 1.0 g Li_2NH (red triangles) at ~585 °C and fitted [4] to a stretched exponential function. The internal reactor temperature *versus* flow comparison is also shown for reference.

Gas Purification

To use this NH_3 -derived hydrogen as a fuel, and to prevent irreparable damage to a PEM fuel cell, the gas stream must be free of trace (<100ppb) levels of unconverted ammonia. Any residual ammonia, an alkaline gas, will damage the acidic Nafion membrane, forming NH_4^+ ions which significantly reduce proton conductivity [11, 12] and therefore the effectiveness and lifetime of the fuel cell. Several approaches for ammonia removal were considered, including dissolution [13] in water, reaction [14] with phosphoric acid to form ammonium phosphates $((\text{NH}_4)_x\text{H}_{3-x}\text{PO}_4)$, adsorption [15] by molecular sieves or activated carbon and complexation [16, 17, 18] with metal halides. Given the objective to design a bench-top demonstrator

and the preference to minimise the volume of the overall system (coupled with safe handling considerations), any aqueous-based absorption methods were dismissed, and neither the molecular sieve nor the activated carbon methodology were pursued. Instead, residual ammonia removal *via* the formation of the magnesium chloride hexaammine complex, $\text{Mg}(\text{NH}_3)_6\text{Cl}_2$, was selected as an effective solid-state approach.

Ammonia is known [19] to form ammine complexes with metal halides, with magnesium chloride being effective and also inexpensive ($\sim\text{US\$ } 150 \text{ tonne}^{-1}$) when compared with other metal halides, e.g. zinc chloride ($\sim\text{US\$ } 950 \text{ tonne}^{-1}$, as at April 2016). As a result, anhydrous magnesium chloride powder was used to fill a column of 19 mm internal diameter, giving a filter bed height of 550–600 mm and thus an average bulk density of $\rho \sim 0.8 \text{ g cm}^{-3}$. For assembly within the integrated system typically two filled columns were set up in parallel to ensure no ammonia slip (*i.e.* escape of trace levels of ammonia through the filter bed) and to allow switching during the experiment to effectively extend the useable operating time. The gas flow was always from the top to the bottom of the column. An initial experiment identified the effective time before ammonia breakthrough to be ~ 80 minutes, detected as an NH_3 signal ($m/z = 17$) by the mass spectrometer, when 1.0 g Li_2NH was present in the reactor at 590°C and 275 sccm NH_3 inlet flow, Fig. 5. This result was taken as a baseline for all subsequent system experiments with the added risk-based assumption that one column could realistically run for half that time, 30–40 minutes, without fear of ammonia slip. Interestingly, water is also detected ($m/z = 18$) in the post-purification gas stream, suggesting that it has been displaced from the MgCl_2 powder within the column, although the levels continuously decrease throughout. The presence of water in the gas stream is a fortuitous and harmless by-product of the chosen purification method, as it can help to maintain the humidity of the fuel cell membrane. The weak NH_3 signal between 33–120 minutes is actually due to the OH^+ fragment from H_2O which also appears at $m/z = 17$.

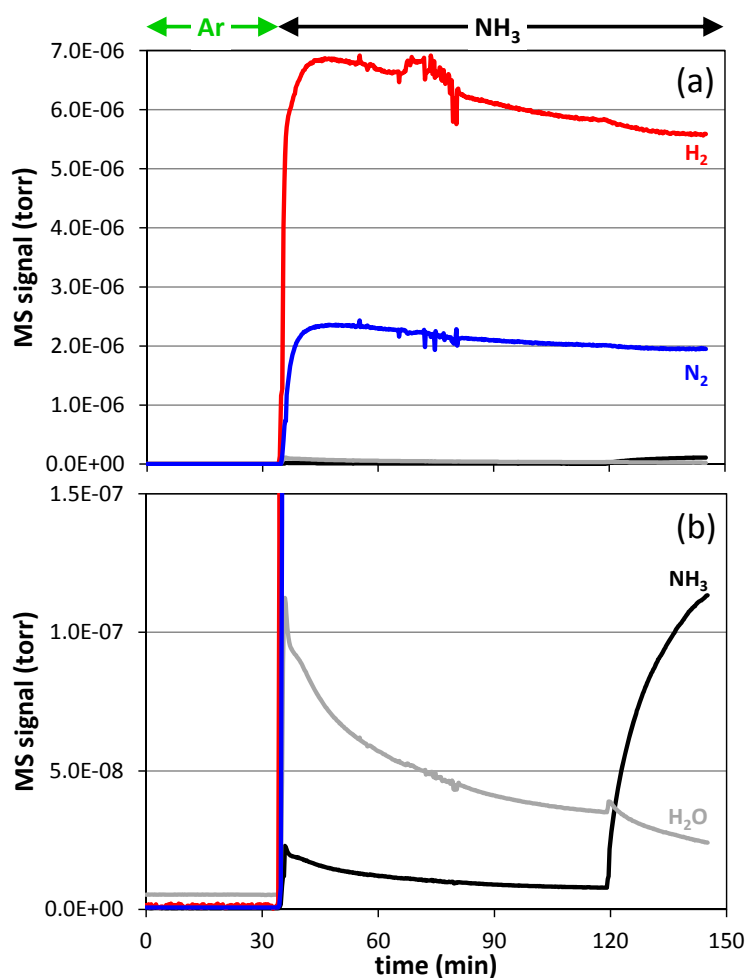


Fig. 5: Determination of ammonia breakthrough from a single MgCl₂-filled column, where the reactor contained 1.0 g Li₂NH and was operated at 590 °C under a 275 sccm NH₃ inlet flow. Plots show mass spectrometer signals for (a) hydrogen and nitrogen and (b) ammonia and water (close-up), after switching from argon to NH₃ gas at 33 minutes.

The absorption of ammonia by the anhydrous MgCl₂ is an exothermic [19] process, equation 2, and so the effect can be seen in the thermal image taken of the top of the powder within the filled column, Fig. 6.



Initially the powder, at ambient temperature, is not easily distinguishable within the thermal image. However, as the column is exposed to the residual ammonia in the gas stream, and the absorption process progresses, heat is released by the MgCl₂ and a distinct front (the highest temperature zone) travels down the filled column. After approximately 20 minutes, this equates to a peak temperature of over 50 °C, with above ambient temperatures observed throughout the top 100–150 mm of the column. In turn, characterisation of the recovered powder allows a semi-quantitative assessment of the amount of ammonia absorbed with respect to the sampling height, Fig. 7, where three samples taken at the top of the column, near the top (~50 mm) and from the bottom of the column are compared to the fresh anhydrous MgCl₂ powder used to fill the column initially. Both ammonia-loaded samples taken from the top of the column show thermogravimetric traces characteristic of Mg(NH₃)_xCl₂ where distinct endothermic events account for approx. 5.8%, 3.0%, and 6.5% weight losses at temperatures 155 °C, 218–232 °C and 363–387 °C, respectively. As anticipated, the near-top sample has a lower overall weight loss than the top sample (14.5% versus 18.5%, respectively). However, the weight loss events occur at the same temperatures, indicating that the same ammine complex (or complexes) has formed although there is less ammonia present overall reflecting that this portion of powder has been exposed to ammonia for a shorter

length of time. The sample from the bottom of the column gives a weight loss trace identical to that of the initial anhydrous MgCl_2 , confirming that no residual ammonia has reached this point in the column and that the purification system works. Interestingly, these small weight loss events (3% and 1.5% at $\sim 260^\circ\text{C}$ and $\sim 500^\circ\text{C}$ respectively) are also seen in the samples taken from the top of the column. This suggests that ammoniation of the entire sample at the top of the column is incomplete, that there may well be gas percolation pathways within the column and that the anhydrous MgCl_2 may not be completely dry. Indeed the detection of traces of H_2O in the QGA data corroborates this third hypothesis, with the stronger ligand strength [20] of NH_3 initiating a displacement of any complexed H_2O molecules and thus release of H_2O into the gas downstream of the purification column.

Overall, anhydrous MgCl_2 is effective at removing residual ammonia from the 75% H_2 / 25% N_2 gas stream. Although further optimisation of this process is possible (e.g. the use of alternative metal halides and supported metal halides as developed by van Hassel *et al.* [18]) and the creation of a simple self-indicating replaceable cartridge-based system would be ideal, this gas purification column arrangement was deemed acceptable for the purposes of this demonstrator and used, as described, in the integrated system.

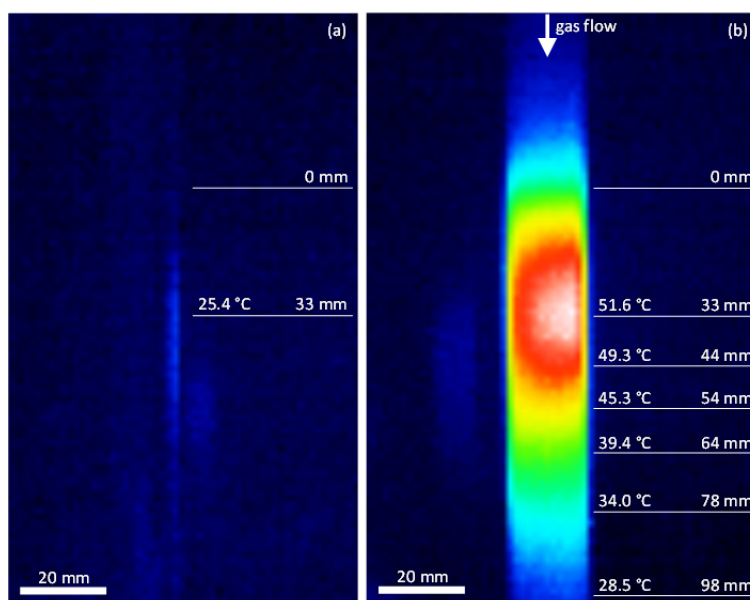


Fig. 6: Thermal images of a MgCl_2 -filled purification column (a) before use and (b) after ~ 20 minutes, showing temperature as a function of powder height whilst residual ammonia is removed from the 75% H_2 / 25% N_2 gas stream.

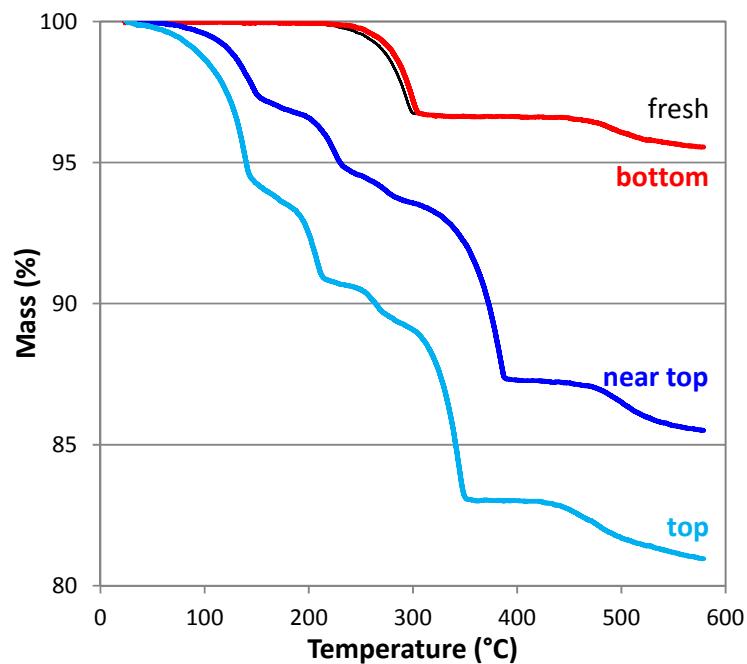


Fig. 7: Thermogravimetric analysis traces showing the decomposition of ammonia-loaded MgCl_2 taken from various heights within a purification column after 50 minutes time on-stream, and compared to the fresh anhydrous MgCl_2 powder.

Fuel Cell Operation

The post-purification gas has a composition of 75% H_2 / 25% N_2 as determined quantitatively by the mass spectrometer. However, given the H-100 PEM fuel cell is designed to operate with a 100% H_2 input, this feed gas composition must be taken into account when operating the fuel cell stack.

Using the Nernst equation a calculation of the maximum possible open-circuit voltage (zero cell current) when 100% H_2 is supplied to the PEM fuel cell gives 1.224 V per cell, and that of the overall 20 cell stack is 24.48 V. If the gas supply is switched to one containing 75% H_2 / 25% N_2 then the equivalent calculation yields 1.221 V per cell, and 24.41 V per 20 cell stack (see SI for detailed calculations). These calculations show that the theoretical loss of stack voltage due to the reduced hydrogen partial pressure in the input gas stream is only 0.07 V; less than 0.3% of the maximum attainable open-circuit potential of the whole stack, if a 100% H_2 feed were used. These values therefore indicate that it should be possible to operate the H-100 fuel cell with the 75% H_2 / 25% N_2 gas mix, however there are further ramifications that also need to be considered.

Purge strategy

Dead-ended anode operation, where the purge valve is only opened for short periods of time, is increasingly used to supply hydrogen to PEM fuel cells [21] as it simplifies the mass flow control of the feed gas (when compared with using a H_2 recirculation pump) whilst also improving fuel efficiency (when compared to running the anode open-ended). During dead-ended anode operation there will always be a drop off in the hydrogen partial pressure along the length of the anode flow field as the H_2 gas is consumed. Simultaneously, an effect known as blanketing [22, 23] can occur, where the build-up of an inert gas (e.g. N_2) effectively blocks the active sites towards the dead-ends of these flow field channels. This, in turn, means that the effective active area of the membrane electrode assembly reduces, and that there is a corresponding impact upon the current generated.

Given the above constraints, a fuel cell controller with programmable flexibility was built that permits modification and optimisation of the purge strategy for use with a 75% H₂ / 25% N₂ gas mix. The controller includes on-board logging and, when connected to a display screen, allows real-time monitoring of stack voltage, current, temperature, pressure as well as any fault conditions that may occur. Although still in the early stages of optimisation the target is to minimise the waste of unused hydrogen gas and maintain an ideal humidity level within the stack channels.

The presence of 25% N₂ in the input gas stream dilutes the hydrogen concentration and has a bearing upon the stack operating in dead-ended anode mode if the purge strategy is sub-optimal. To develop an appropriate strategy it was decided to initially run the fuel cell stack open-ended, with a load of 5 A (68 W) using the 75% H₂ / 25% N₂ gas mix. This confirmed that the fuel cell stack was working correctly and, through measurement of the voltage across each cell, that all the cells were uniformly similar (within a 30 mV range) and that no mass transport losses (reactant starvation) exist at the furthest extremity of the stack (see SI). A scope probe was also connected to this furthest extremity cell (the cell most likely to be affected by H₂ starvation) and the stack run at 8.7 A (100 W) open-ended. It showed that the baseline steady-state single cell voltage was 600 mV within this humidified membrane electrode assembly (MEA) operating at ~40 °C, measured after the stack had been running for approximately 1 hour. Subsequently the post-stack purge valve was closed and the decay in the cell voltage monitored (i.e. dead-ended anode operation). This determined that the cell voltage only starts to decay after 1.7 s, and that following a drop of more than 200 mV, it took 120 ms for the voltage to recover to the original 600 mV level after the purge valve as re-opened (see SI). Overall, therefore, it was established that, at an operating point of 8.7 A (100 W), a purge interval of 1.7 s and a purge duration of 120 ms would allow continuous operation of the stack.

Careful adjustment of these values was required in order to create a purge algorithm that is suitable for sub-optimal conditions (e.g. start-up when cold, dry stack after a period of non-operation). Consequently a cautious approach was chosen, whereby for nominal power operation at 8.7 A (100 W) both the purge interval was halved and also the purge duration was doubled, to 800 ms and 240 ms, respectively. For zero load (0 A) conditions, no hydrogen is consumed, however the hydrogen partial pressure at the anode gradually decreases due to membrane cross-over. To avoid fuel starvation when an electrical load is applied, a zero load purge was implemented, with a purge interval of 4 s and a purge duration of 100 ms. In combination with the nominal power conditions these values were used to create a dynamic purge strategy algorithm within the custom-built controller. Using a linear relationship between zero load and nominal power, and extrapolating for higher currents, these *cautious* purge strategy relationships are given in equations 3 and 4:

$$\text{Purge interval (s)} = 4 \text{ s} - \left(3.2 \text{ s} \times \frac{\text{Current (A)}}{8.7 \text{ A}} \right) \quad (3)$$

$$\text{Purge duration (ms)} = 100 \text{ ms} + (140 \text{ msA}^{-1} \times \text{Current (A)}) \quad (4)$$

In particular, this purge duration protocol allows for a change of the bulk gas and also for diffusion of nitrogen and hydrogen to the reaction sites. Overall, the dead-ended purge strategy was developed to reduce the risk of fuel starvation at the anode (and closing the purge valve earlier may in fact achieve the same effect), however it is sub-optimal in terms of efficiency, with an excess of hydrogen still being purged. At this stage in the assembly of an integrated demonstrator system this trade-off is acceptable. Further purge strategy optimisation is on-going. A secondary function of the purge strategy is to regulate the water management within the stack. Given that the H-100 fuel cell has a self-humidifying MEA, a change in the purge strategy could well alter the ideal proton conductivity conditions present; either too humid or too

dry and the electrochemically active surface area decreases thereby hindering gas diffusion. The impact of the new dynamic purge strategy upon humidity within the MEA over time is also currently being considered.

System Performance

Using the custom-built fuel cell controller, with its dynamic purge control strategy, the PEM fuel cell operates by dosing defined volumes of the 75% H₂ / 25% N₂ gas mix into the stack. However, the combination of a small gas volume between the pressure regulator and the fuel cell, along with the low flow rate achievable through the regulator (in comparison to the purge cycle demands) caused a dramatic reduction in the pressure, sufficient for the fuel cell 'low system pressure' error to trip. To overcome this, a 1 litre buffer volume was inserted between the gas regulator and the supply valve in order to increase the post-regulator volume and thus dampen any effects that the dosing strategy has upon the gas pressure. Additionally, the gas regulator is required to consistently deliver 350–650 mbar overpressure to the fuel cell. A 4 litre buffer volume was, therefore, inserted upstream of the gas regulator to increase the volume of gas pressurised at ~2 bar such that the regulator could operate effectively and maintain the fine control needed. If less than 350 mbar was available a 'low system pressure' error appears and the fuel cell stops working; if more than 650 mbar is delivered then the likelihood of perforating the membrane increases which would irreparably damage the fuel cell. Together, these buffer volumes successfully removed any fuel cell pressure errors and established a smooth supply of the hydrogen-containing gas, at ~0.5 bar overpressure, to the fuel cell stack.

Assembling each component in series, such that the hydrogen produced from the decomposition of ammonia is used to power a PEM fuel cell, leads to the performance characteristics that are shown in Fig. 8. With the reactor containing 1.0 g Li₂NH, and thus giving more than 98% ammonia conversion at 300 sccm, the purified 75% H₂ / 25% N₂ gas mixture was used to initially increase the pressure in the fuel cell gas handling line (10 min) and then also self-pressurise the 4L buffer volume (14 min). When the pressure nears 2 bar, the ammonia gas flow to the reactor was increased in steps (23–35 min) to avoid blowing the catalyst out of the reactor and to increase hydrogen production. This increased flow simultaneously cools the reactor thus the furnace set point was raised by 10–15 °C to compensate for this and maintain the catalyst at an optimal 585 °C working temperature. During operation, the system pressure in the reactor and purification columns was kept at ~1800 mbar to ensure sufficient upstream pressure to consistently deliver the ~0.5 bar overpressure required by the fuel cell. At a 20 W power load, this required a 325 sccm ammonia inlet flow to the reactor; however, at 30 W and 40 W flows of 375 sccm and 500 sccm were needed, respectively. When running the fuel cell, the power load dictates the level of voltage and current drawn, with the purge interval decreasing in line with the increased demand for hydrogen, Table 1. The gas handling system was effective at handling the overpressure demands and although the stack operating temperature increases by 4 °C, as the load increases, it was well within its working range throughout. In such a relatively short test, the humidity of the fuel cell is less of a concern. However, any trace amounts of water displaced during purification will be entrained within the gas stream and thus delivered to the fuel cell membrane to aid and/or maintain its humidity. During full operation of the whole system, a 27 W LED television was switched on and run effectively using the hydrogen supplied to the PEM fuel cell as a result of the catalytic decomposition of ammonia gas.

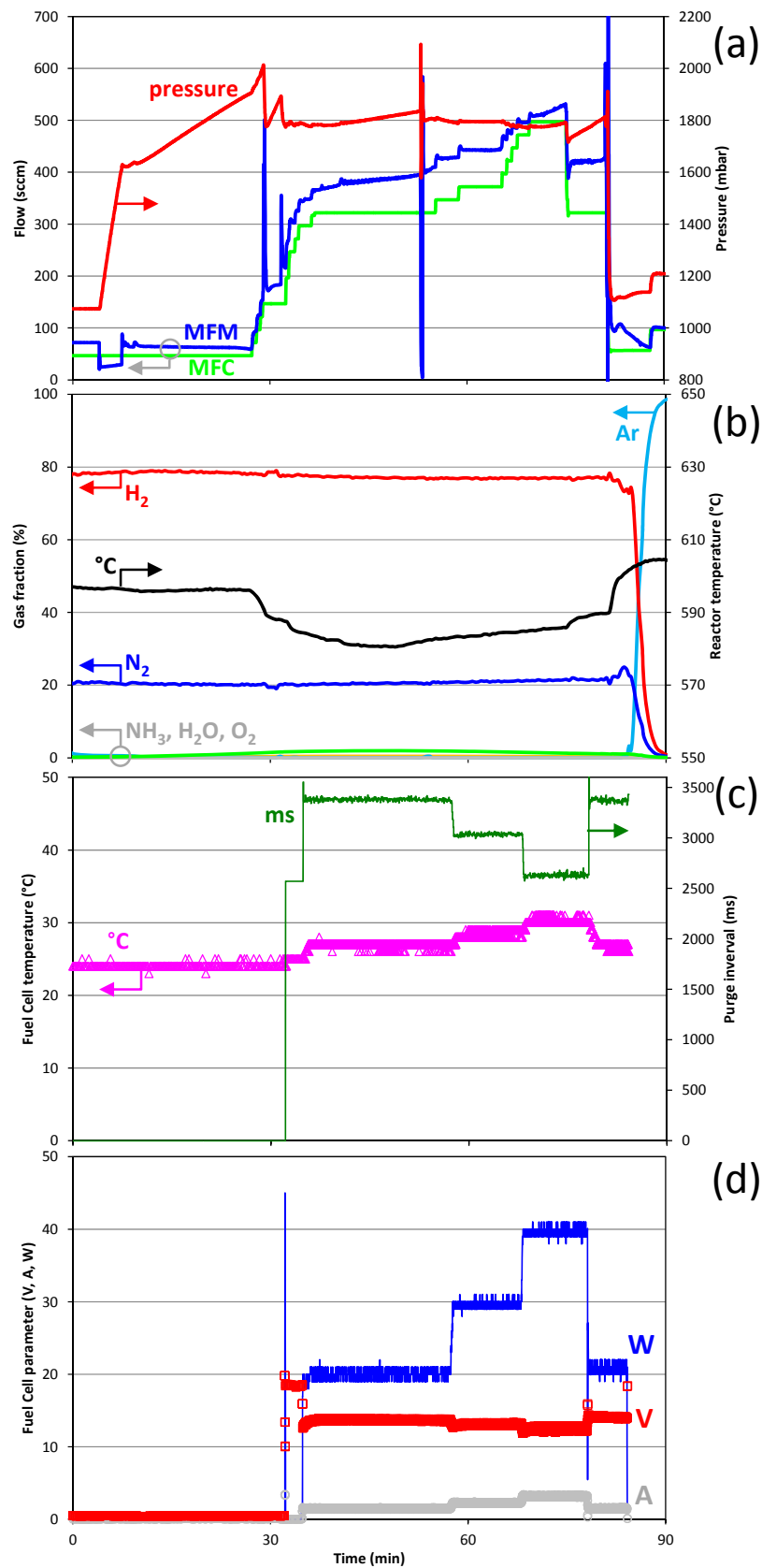


Fig. 8: Time aligned demonstrator system data showing (a) reactor flow conditions, (b) gas composition and reactor temperature, (c) fuel cell parameters (temperature and purge interval) and (d) fuel cell parameters (power, voltage and current). Note: the spike in (a) at 52 minutes run time is caused by the purification column switching process.

Power load (W)	0	20	30	40
Voltage (V)	0	13.6	13.0	12.4
Current (A)	0	1.4	2.3	3.2
Purge interval (ms)	0	3385	3042	2636
Temperature (°C)	24	27	29	31
Overpressure (mbar)	583	470	448	388

Table 1: H-100 fuel cell parameters when in use within the integrated demonstrator.

Summary

Light metal amides and imides have been identified [3, 4, 5] to be effective at decomposing ammonia into its constituents, hydrogen and nitrogen. Here, we show that this catalytic reaction can be harnessed within a bench-top demonstrator which produced 40 W from a PEM fuel cell. For this process, lithium imide, Li_2NH , was chosen as the ammonia decomposition catalyst as it is both highly active and solid at the selected 585 °C operating temperature. The post-reaction gas is predominantly a 75% H_2 / 25% N_2 mix; however traces of unreacted ammonia are also present. Importantly, to be able to use this gas to feed a PEM fuel cell, it is imperative that it is ammonia-free, and we show that anhydrous MgCl_2 is effective at scavenging this residual ammonia. The presence of 25% N_2 in the post-purification gas stream, though, has further consequences for the operation of the fuel cell as nitrogen is known to have a ‘blanketing’ effect, essentially blocking the active sites in the fuel cell membrane. As a result, a dynamic purge strategy was created that accommodated the 75% H_2 / 25% N_2 gas stream without causing long-term damage to the PEM fuel cell. Fully assembled, the bench-top system was able to power a television thereby delivering a first demonstrator for this innovative hydrogen production method, based upon light metal amide-imides, and, in so doing, achieving a significant milestone in the development of a fully integrated heat and mass balanced system for eventual use in environmentally sustainable transport or off-grid applications.

Glossary

AC = alternating current

DC = direct current

i.d. = internal diameter

LED = light emitting diode

MEA = membrane electrode assembly

MFC = mass flow controller

MFM = mass flow meter

PEM = proton exchange membrane

References

1	E. Kroch, <i>J. Inst. Petrol</i> , 1945, 31 , pp213-223. "Ammonia — a fuel for motor buses"
2	G. Thomas and G. Parks, "Potential Roles of Ammonia in a Hydrogen Economy"; U.S. Department of Energy: Washington, DC, 2006, pp 1–23.
3	J. W. Makepeace, T. J. Wood, H. M. A. Hunter, M. O. Jones and W. I. F. David, <i>Chem. Sci.</i> , 2015, 6 , pp3805-3815. "Ammonia decomposition catalysis using non-stoichiometric lithium imide"
4	W. I. F. David, J. W. Makepeace, S. K. Callear, H. M. A. Hunter, J. D. Taylor, T. J. Wood and M. O. Jones, <i>J. Am. Chem. Soc.</i> , 2014, 136 , pp13082–13085. "Hydrogen Production from Ammonia using Sodium Amide"
5	J. W. Makepeace, H. M. A. Hunter, T. J. Wood, R. I. Smith, C. A. Murray, W. I. F. David, <i>Faraday Discuss.</i> , 2016, 188 , pp525-544. "Ammonia decomposition catalysts using lithium-calcium imide"
6	T. Hejze, J.O. Besenhard, K. Kordesch, M. Cifrain and R. R. Aronsson, <i>J Power Sources</i> , 2008, 176 , pp490-493. "Current status of combined systems using alkaline fuel cells and ammonia as a hydrogen carrier"
7	M. L. Perry and T. F. Fuller, <i>J. Electrochem. Soc.</i> , 2002, 149 (7), ppS59-S67. "A Historical Perspective of Fuel Cell Technology in the 20 th Century"
8	F. A. Uribe, S. Gottesfeld and T. A. Zawodzinski, Jr., <i>J Electrochem Soc.</i> , 2002, 140 , ppA293-A296. "Effect of Ammonia as Potential Fuel Impurity on Proton Exchange Membrane Fuel Cell Performance"
9	Y. H. Hu and E. Ruckenstein, <i>Ind. Eng. Chem. Res.</i> , 2006, 45 , pp4993-4998. "Ultrafast reaction between Li ₃ N and LiNH ₂ to prepare the effective hydrogen storage material Li ₂ NH"
10	W. I. F. David, M. O. Jones, D. H. Gregory, C. M. Jewell, S. R. Johnson, A. Walton and P. P. Edwards, <i>J. Am. Chem. Soc.</i> , 2007, 129 , pp1594–1601. "A mechanism for non-stoichiometry in the lithium amide/lithium imide hydrogen storage reaction"
11	R. Halseid, P. J. S. Vie and R. Tunold, <i>J. Power Sources</i> , 2006, 154 , pp343-350. "Effect of ammonia on the performance of polymer electrolyte membrane fuel cells"
12	H. J. Soto, W-K. Lee, J. W. Van Zee and M. Murthy, <i>Electrochemical and Solid-State Letters</i> , 2003, 6 (7), ppA133-135. "Effect of Transient Ammonia Concentrations on PEMFC Performance"
13	L. J. Bonville Jr.; N. E. Cipollini, J. Garow, R. R. Lesieur, D. F. Szydlowski, Z. D. Vance and D. J. Wheeler, U.S. Patent 6,376,114 (2002) "Reformate fuel treatment system for a fuel cell power plant"
14	M. Katz, G. A. Gruver and H. R. Kunz, U.S. Patent 4,259,302 (1981) "Regenerable Ammonia Scrubber"
15	G. P. Holland, B. R. Cherry and T. M. Alam, <i>J. Phys. Chem. B</i> , 2004, 108 , pp16420-16426. "15N Solid-State NMR Characterization of Ammonia Adsorption Environments in 3A Zeolite Molecular Sieves"
16	C. C. Rodrigues, D. de Moraes Jr, S. W. da Nóbrega and M. G. Barboza, <i>Bioresour. Technol.</i> , 2007, 98 (4), pp886-891. "Ammonia adsorption in a fixed bed of activated carbon"
17	T. J. Badosz and C. Petit, <i>J. Colloid Interface Sci.</i> , 2009, 338 (2), pp329-345. "On the reactive adsorption of ammonia on activated carbons modified by impregnation with inorganic compounds"
18	B. A. van Hassel, J. R. Karra, J. Santana, S. Saita, A. Murray, D. Goberman, R. Chahine and D. Cossement, <i>Sep. Purif. Technol.</i> , 2015, 142 , pp215–226. "Ammonia sorbent development for on-board H ₂ purification"
19	M. O. Jones, D. M. Royse, P. P. Edwards and W. I. F. David, <i>Chem. Phys.</i> , 2013, 427 , pp38-43. "The structure and desorption properties of the amines of the group II halides"
20	P. Atkins, T. Overton, J. Rourke, M. Weller and F. Armstrong, Shriver and Atkins' Inorganic Chemistry, 2010, 5 th Ed, Chapter 20, Oxford University Press, Oxford, UK. "d-Metal complexes: electronic structure and properties"
21	Q. Meyer, S. Ashton, O. Curnick, T. Reisch, P. Adcock, K. Ronaszegi, J. B. Robinson and D. J. L. Brett, <i>J. Power Sources</i> , 2014, 254 , pp1-9. "Dead-ended anode polymer electrolyte fuel cell stack operation investigated using EIS, off-gas analysis and thermal imaging"
22	J. Yu, Z. Jiang, M. Hou, D. Liang, Y. Xiao, M. Dou, Z. Shao and B. Yi, <i>J. Power Sources</i> , 2014, 246 , pp90-94. "Analysis of the behavior and degradation in proton exchange membrane fuel cells with a dead-ended anode"
23	J. B. Siegel, S. V. Bohac, A. G. Stefanopolou and S. Yesilyurt, <i>J. Electrochemical Soc.</i> , 2010, 157 (7),

ASSOCIATED CONTENT

Supporting Information

X-ray diffraction pattern of Li_2NH , FTIR spectra of $\text{Mg}(\text{NH}_3)_x\text{Cl}_2$ purification column residues and fuel cell voltage calculations and test results.

AUTHOR INFORMATION

Corresponding Author

hazel.hunter@stfc.ac.uk

Notes

The authors declare no competing financial interest.

Acknowledgments

The authors acknowledge the technical assistance of James Taylor for laboratory management, and thank Kate Ronayne, Beth Evans, and Steven Wakefield for project management and useful guidance. This work was financially supported by an STFC Innovations Proof of Concept Award (Phase 3 POCF1213-14).

Supplementary Information

Demonstrating hydrogen production from ammonia with an imide catalyst – powering a small proton exchange membrane fuel cell

Hazel MA Hunter^{1*}, Joshua W Makepeace², Thomas J Wood¹, O Simon Mylius³, Mark G Kibble¹,
Jamie B Nutter¹, Martin O Jones¹ and William IF David^{1,2}

¹ISIS Facility, STFC Rutherford Appleton Laboratory, Harwell Campus, Didcot, OX11 0QX, UK.

²Inorganic Chemistry Laboratory, University of Oxford, South Parks Road, Oxford, OX1 3QR, UK

³Arcola Energy Ltd, 24 Ashwin Street, Dalston, London E8 3DL, U.K.

* Corresponding author: hazel.hunter@stfc.ac.uk

Contents

Section	Page
XRD of synthesised lithium imide catalyst	S1
Purification column FTIR characterisation	S2
Fuel Cell Operation	S3

XRD of synthesised lithium imide catalyst

Powder X-ray diffraction patterns were collected on a PANalytical X'Pert diffractometer operating at 45 kV using Cu K α_1 radiation ($\lambda = 1.54051$ Å, Ge (111) monochromator). The synthesised Li₂NH sample was mounted as a thin film on a glass slide, within an air sensitive sample holder possessing a polyvinyl acetate window, and the data were collected between 10 –85 °2 θ over 1 hour. TOPAS-Academic¹ (v5) was used to identify the phases present by Rietveld analysis.

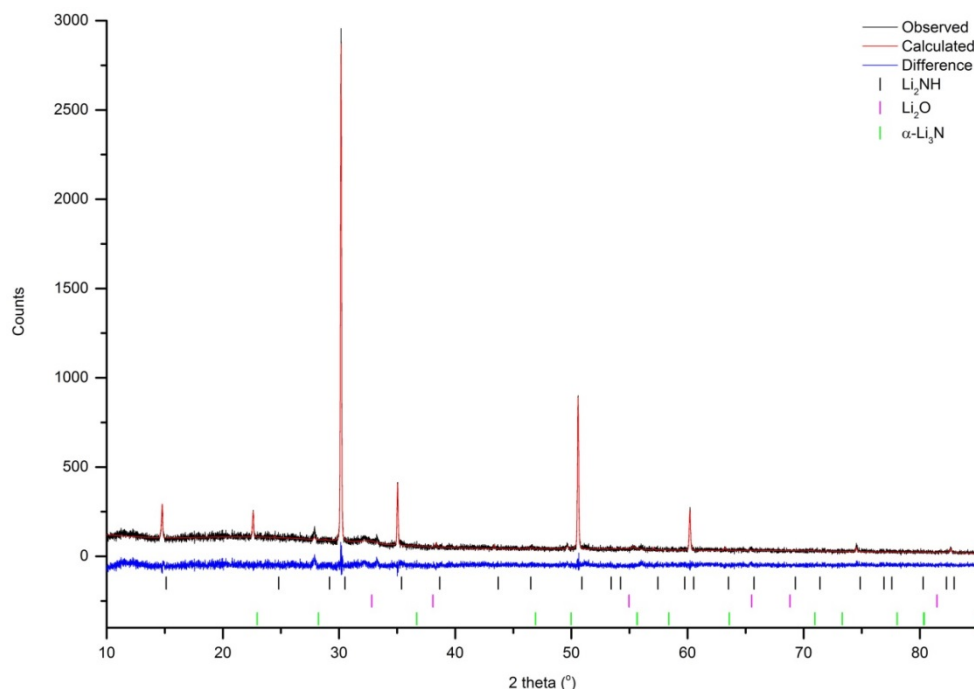


Fig. S1: Powder X-ray diffraction pattern, with refinement, for the synthesised Li₂NH material.
Calculated composition (wt%): 96.0% Li₂NH, 1.5% Li₃N and 2.5% Li₂O.

Reference:

1: A Coelho, TOPAS-Academic, v5, Coelho Software: Brisbane, Australia, 2012; <http://topas-academic.net/>

Purification column FTIR characterisation

The infrared spectra were collected on a Bruker VERTEX 70 spectrometer equipped with a Bruker Platinum ATR and operated *via* Bruker OPUS (v7.0) software. The powder was placed on the ATR assembly and an appropriate force applied to ensure effective contact with the crystal. The absorbance spectra were averaged over 32 scans, collected at 2 cm^{-1} wavenumber resolution, between 4000 and 400 cm^{-1} .

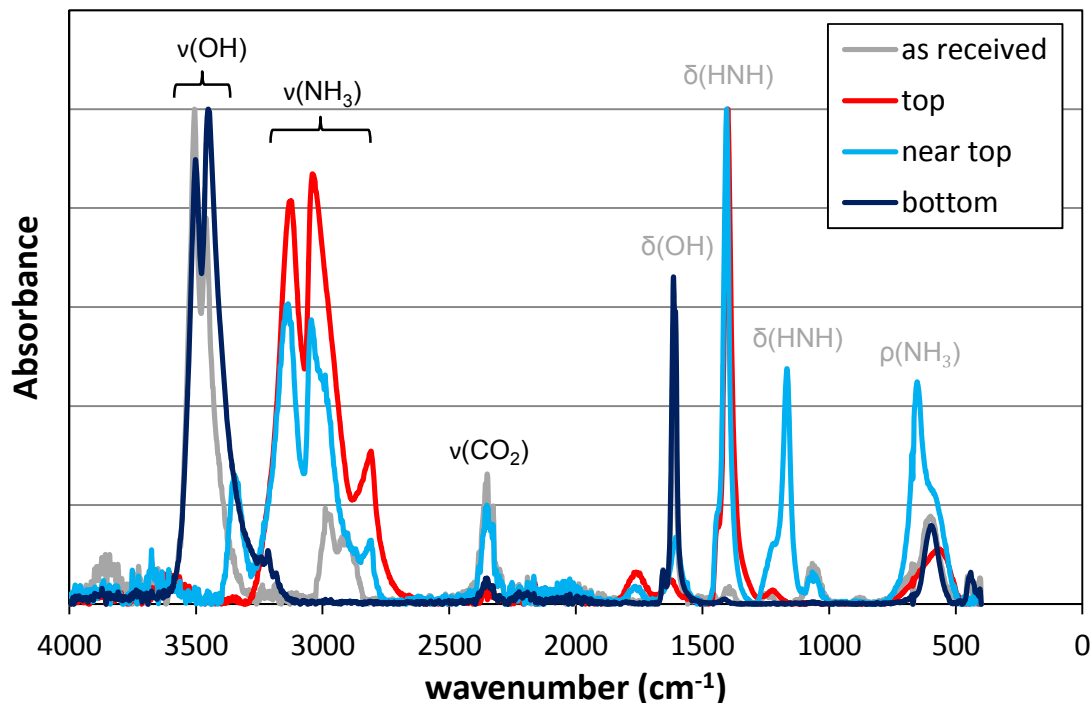


Fig. S2: Normalised FTIR spectra for solids recovered from the top, near top and bottom of the purification column, in comparison to that of the fresh MgCl_2 material, with tentative peak assignments shown.

Fuel Cell Operation

Nernst Equation

The maximum possible open-circuit voltage (zero cell current) is a function of the temperature and the partial pressure of the reactants, as described by the Nernst equation (equation S1):

$$E = E^{\circ} - \frac{RT}{nF} \ln \left[\frac{a_{\text{products}}}{a_{\text{reactants}}} \right] = E^{\circ} - \frac{RT}{nF} \ln \left[\frac{a_{\text{H}_2\text{O}}}{a_{\text{H}_2} \times (a_{\text{O}_2})^{1/2}} \right] \quad (\text{S1})$$

where E is the open-circuit potential (V) of a single cell, E° is the cell potential under standard conditions (1.229 V), R is the ideal gas constant ($8.314 \text{ J K}^{-1} \text{ mol}^{-1}$), T is the operating temperature in Kelvin (298 K), n is the number of electrons transferred in the balanced equation of the reaction (2 electrons), F is the Faraday constant (96485 C mol^{-1}), and a is the activity. The activity can be further described as

$$a_i = \frac{P}{P^{\circ}} y_i \quad (\text{S2})$$

where P is the pressure at the electrode, P° is the reference pressure and y_i is the mole fraction.

The H-100 PEM fuel cell is designed for use with a 100% H_2 input gas stream at 1.5 bar, and with air (*i.e.* 21% O_2) on the cathode side. As a result the open circuit potential for a single cell at 298 K can be calculated:

$$E = 1.229 - \frac{8.314 \times 298}{2 \times 96485} \ln \left[\frac{1}{1.5 \times (0.21)^{1/2}} \right] = 1.224 \text{ V} \quad (\text{S3})$$

And, given that the H-100 stack is composed of 20 cells, the overall stack potential is 24.48 V. However, the actual gas supplied to the anode is a 75% H_2 / 25% N_2 mixture, thus the partial pressure of H_2 is reduced to $0.75 \times 1.5 = 1.125$ bar. Consequently, the open-circuit potential of a single cell at 298 K is:

$$E = 1.229 - \frac{8.314 \times 298}{2 \times 96485} \ln \left[\frac{1}{1.125 \times (0.21)^{1/2}} \right] = 1.221 \text{ V} \quad (\text{S4})$$

and that of the overall stack is 24.41 V. These calculations show that the theoretical loss of stack voltage due to the reduced hydrogen partial pressure in the input gas stream is only 0.07 V; less than 0.3 % of the maximum attainable open-circuit voltage of the whole stack, if a 100% H_2 feed were used. This calculation indicates that it should theoretically be possible to operate the H-100 fuel cell with the 75% H_2 / 25% N_2 gas mix.

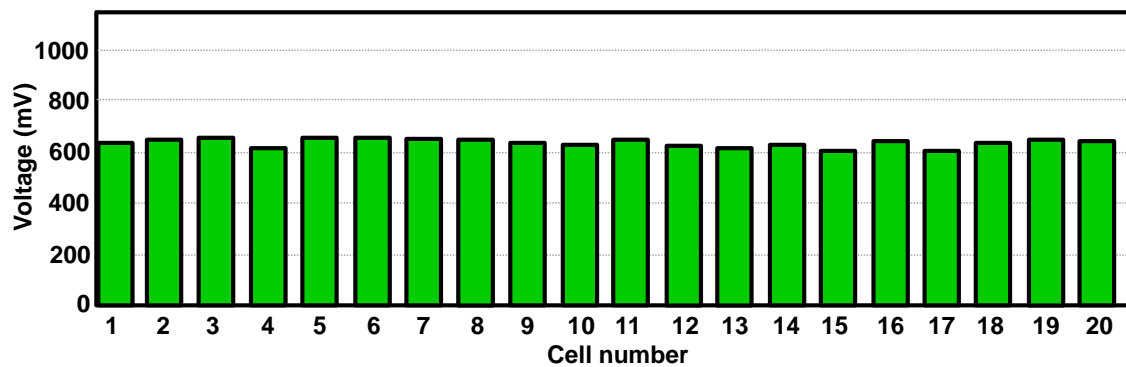


Fig. S3: Cell voltage measurements across the 20 cells of the H-100 PEM fuel cell stack, operating at 5 A using the 75% H_2 / 25% N_2 gas mix. All the cells are within a 30 mV range.

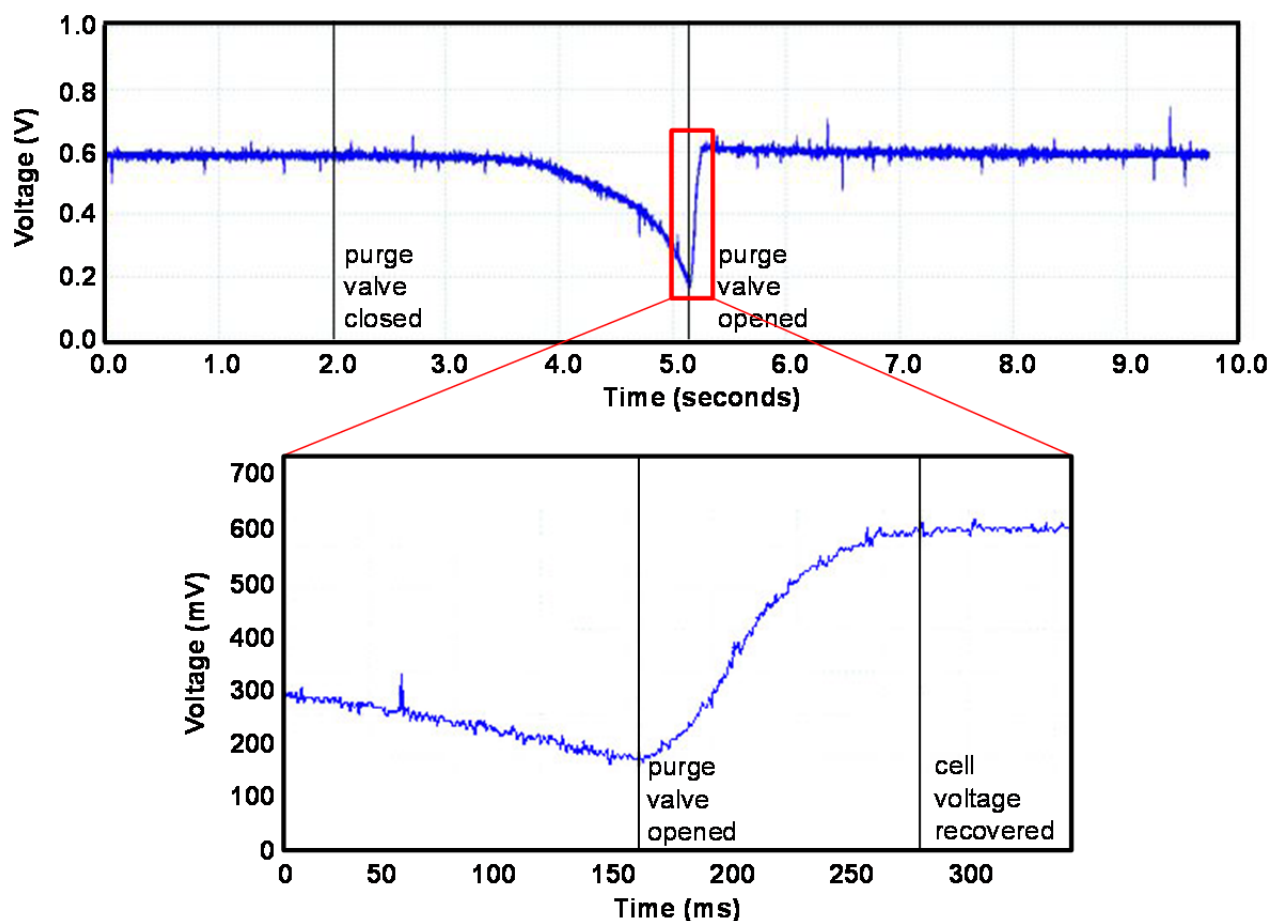


Fig. S4: Monitoring the cell voltage decay after closing the purge valve, with expanded section showing the cell voltage recovery after opening the purge valve; H-100 fuel cell operating at 100 W using the 75% H₂ / 25% N₂ gas mix.

Description	Value
Cell count	20
Nominal Current	8.5 A
Max. Current	10.0 A
Purge Duration No Load	0.10 s
Purge Duration Max. Current	0.25 s
Purge Interval No Load	4.00 s
Purge Interval Nominal Current	0.80 s
Min. Pressure	0.348 bar
Max. Pressure	0.648 bar

Table S1: H-100 fuel cell control parameters developed for use with a 75% H₂ / 25% N₂ gas mix feedstock. Abbreviations: Min. = minimum; Max. = maximum.